Geophysical Research Letters

RESEARCH LETTER
10.1029/2019GL083894

Regional Climate Effects of Biomass Burning and Dust in East Asia: Evidence From Modeling and Observation

Xinyi Dong[1], Joshua S. Fu[1,2,3], Kan Huang[1,4], Qingzhao Zhu[1], and Matthew Tipton[1]

[1]Department of Civil and Environmental Engineering, The University of Tennessee, Knoxville, TN, USA, [2]Climate Change Science Institute, Oak Ridge National Laboratory, Oak Ridge, TN, USA, [3]Department of Atmospheric Sciences, National Central University, Taoyuan, Taiwan, [4]Center for Atmospheric Chemistry Study, Department of Environmental Science and Engineering, Fudan University, Shanghai, China

Key Points:
- Peninsular Southeast Asia biomass burning shows larger warming effect (10-20 W/m^2) over downwind region than over the source area (5-10 W/m^2)
- Dust shows a cooling effect of up to -9 W/m^2 with a few exceptions along north and east edges of Tibet Plateau due to snow or ice cover
- Dust and biomass burning cool the near surface air and warm the upper air, and their radiative efficiencies decrease during transport

Supporting Information:
- Supporting Information S1

Correspondence to:
J. S. Fu,
jsfu@utk.edu

Citation:
Dong, X., Fu, J. S., Huang, K., Zhu, Q., & Tipton, M. (2019). Regional climate effects of biomass burning and dust in East Asia: Evidence from modeling and observation. *Geophysical Research Letters*, *46*, 11,490–11,499. https://doi.org/10.1029/2019GL083894

Received 27 MAY 2019
Accepted 5 SEP 2019
Accepted article online 9 SEP 2019
Published online 28 OCT 2019

Abstract This study integrates data from regional model simulations, reanalysis data set, radiosonde observations, lidar measurements, and satellite products to evaluate the direct radiative forcing effect of biomass burning and dust over East Asia. During March and April, we find an overall cooling effect of the dust of −5 to −9 W/m^2. Biomass burning aerosols from Peninsular Southeast Asia exhibit a warming effect of 5–10 W/m^2 over the source area, lower than that over the downwind area of 10–20 W/m^2 because of significantly higher cloud coverage in South China. Dust and biomass burning aerosols are found to cool the near surface layer (0–1 km) by −0.5 and −0.3 K, respectively, and warm the upper air (1–5 km) by +0.1 and +0.2 K, respectively. In Taipei, simultaneous presences of dust and biomass burning lead to cooling of near-surface air by −1.5 K and warming of upper air by +1 K.

Plain Language Summary Biomass burning and dust are the largest natural emission sources of atmospheric aerosol. However, no solid consensus exists regarding whether biomass burning or dust contributes to a net warming or cooling effect. This study integrates data from regional climate model simulations, reanalysis data, radiosonde observations, lidar measurements, and satellite products to evaluate the climate effects of biomass burning and dust at a regional scale over East Asia. We find prominent warming effects by biomass burning in Peninsular Southeast Asia, which is more significant over the downwind area in South China than over the emission source area. Dust exhibits cooling effects, with a few exceptions over areas covered by semipersistent snow or ice. We also reveal that under conditions in which both biomass burning and dust aerosols are present, they exhibit an overall slight warming effect.

1. Introduction

Biomass burning and wind-blown dust are the two most important natural emission sources of atmospheric aerosol, which directly alters the radiative forcing (RF) budget and indirectly affects the atmospheric energy balance through interactions with clouds. However, the climate effects of these aerosol sources are poorly constrained, and it is still uncertain whether biomass burning has a net warming or cooling effect on global climate. The Intergovernmental Panel on Climate Change has reported the global mean RF of biomass burning aerosol as −0.2 W/m^2 in its Third Assessment Report, +0.03 ± 0.12 W/m^2 in its Fourth Assessment Report, and effectively 0 (−0.2–+0.2 W/m^2) in its Fifth Assessment Report (AR5). Quantification of biomass burning climate effects suffers from uncertainties in emission factors, identification of small fires, fire plume injection height, and optical properties. Biomass burning emits various types of aerosols with opposing radiative effects, such as strongly warming aerosols like black carbon (BC) and strongly cooling aerosols like sulfate. Field measurements indicate that biomass burning aerosol mass contributions of different types of burning activities can vary by a factor of 2 for black carbon and a factor of 10 for inorganic aerosol (Akagi et al., 2011). Some pilot studies have investigated the impact of biomass burning on regional climate, but most of these research efforts have focused on South America (Kaufman & Koren, 2006; Koren et al., 2008) and Africa (Haywood et al., 2003; Keil & Haywood, 2003; Wilcox, 2012), while East Asia is less studied and documented. Additionally, although biomass burning injection height is usually limited to within the boundary layer (Reid et al., 2009), studies over Peninsular Southeast Asia (PSEA) suggested that aerosols in this region could be uplifted into the free troposphere above stratocumulus clouds (Dong & Fu, 2015b; Hsu et al., 2003). Therefore, the subsequent absorbing aerosol above clouds in PSEA may exhibit different RF effects as compared to biomass burning aerosol elsewhere (N. H. Lin et al., 2013; Tsay et al., 2013, 2016).

Knowledge of the climate effects of dust is comparatively well developed (Gu et al., 2006, 2016), but no solid consensus regarding these effects has been established due to substantial diversity in estimations of atmospheric dust loading and size distribution. Multimodel comparisons reveal that simulated dust PM_{10}, surface concentration, and aerosol optical depth (AOD) vary by factors of 5, 10, and 2, respectively (Huneeus et al., 2011), due to variations in emission and size distribution schemes. Fourth Assessment Report reported the net RF of dust falls between −0.3 and +0.1 W/m^2 (Forster & Taylor, 2006) but also indicated that top-of-atmosphere dust may exhibit an extremely strong instantaneous shortwave direct radiative effect (DRE) of up to −130 W/m^2 over the West African coast (Haywood et al., 2003; Hsu et al., 2000). AR5 reported the RF of dust as -0.14 ± 0.11 W/m^2, suggesting an overall cooling effect. However, a recent study suggests current models substantially overestimate the fine (<2 μm) fraction of dust particles and reports observation constrained model estimated dust DRE between −0.48 and +0.2 W/m^2, which suggests a potential net warming effect of dust (Kok et al., 2017). Furthermore, AR5 categorizes the understanding of dust loading as "low confidence" due to substantial diversity in estimated future changes, ranging from 300% increase (Woodward et al., 2005) to 60% decrease (Mahowald et al., 2006) from current status.

This study employs the Weather Research and Forecasting/Community Multiscale Air Quality (WRF/CMAQ) modeling system, satellite products, and radiosonde observations to estimate the DRE of biomass burning and dust over East Asia and investigates their combined impact under coexist aerosol conditions for the first time. The integrated analysis demonstrates the surface cooling and upper air warming effects of biomass burning and dust aerosols and reveals the urgent need to improve cloud simulation in regional modeling systems to more accurately estimate aerosol climate impacts.

2. Methods

CMAQ v5.0.1 and the WRF v3.4 were applied in this study in a two-way mode with the Rapid Radiative Transfer Model for global circulation model (GCM) to estimate aerosol RF (Wong et al., 2012), which include the representation of direct effect only (Appel et al., 2017; Gan et al., 2015). We applied the Global Fire Emission Database v4.1s (van der Werf et al., 2017) for biomass burning emission and the improved wind-blown dust scheme with source-dependent mineralogical distribution mechanism (Dong et al., 2016) implemented in the two-way mode WRF/CMAQ model for dust emission; detailed discussions of the emission inputs and model mechanisms are reported in Dong et al. (2016). Simulations were conducted over five consecutive years from 2006 through 2010 for March and April to account for the PSEA biomass burning season and East Asia spring dust storms. Scenarios with and without biomass burning and scenarios with and without wind-blown dust were simulated to isolate the impacts of each aerosol source. The change of upward shortwave radiation flux at top of atmosphere between them was used to represent the aerosol DRE (Heald et al., 2014). Multiple satellite products are utilized to evaluate WRF/CMAQ simulated shortwave radiation flux and temperature and relative humidity at eight vertical layers from 1,000 to 500 hPa, as shown in the supporting information (Figures S1–S5 and Tables S1–S4) for which no obvious systematic bias or significant uncertainties are identified.

Huang et al. (2018) used the bias between reanalysis data and sounding data as an indicator to demonstrate the impact of intensive anthropogenic aerosol on temperature profile at Beijing. In this study, we also adopt this method to probe into the influences of dust and biomass burning aerosol. We derive the bias between sounding observations and reanalysis data during episodes with and without the presence of dust and biomass burning, respectively, and calculate the HD-Index (Huang et al., 2018) as

$$\mathrm{HD-Index} = \frac{\sum_{i=1}^{n}|\Delta \mathbf{T_i}|}{n} + \frac{\sum_{j=1}^{m}|\Delta \mathbf{T_j}|}{m},$$

where n and m are the numbers of pressure layers where aerosols exhibit dimming and warming effects, respectively, and $\Delta \mathbf{T_i}$ and $\Delta \mathbf{T_j}$ are the temperature bias between observation and reanalysis data, respectively. Since reanalysis products usually do not consider the aerosol feedback, the bias during excess aerosol episodes should be significantly larger than the bias during episodes without excessive aerosol loading. This method allows a prompt investigation of long-term aerosol climate effect with archived reanalysis and observation data, but it shall be noted that the HD-Index has no physical meaning. In addition, reanalysis data are subject to the same uncertainties inherent in the source model, so the bias between observations and reanalysis data

depicts the overall discrepancies and cannot be completely attributed to the aerosol feedback. In this study, the air temperature profiles are collected from the Integrated Global Radiosonde Archive (IGRA) of sounding measurements provided by the National Climate Data Center (NCDC) and reanalysis data is collected from the ERA-Interim dataset provided by the European Centre for Medium-Range Weather Forecasts (ECMWF). It shall be noticed that WRF/CMAQ only includes the direct and semidirect effects, while indirect effect were probed with the HD-Index method since the reanalysis data considered neither of them.

3. Results and Discussion

3.1. Impact of Biomass Burning on Regional Climate

Impacts of PSEA biomass burning aerosol on RF and air temperature are presented in Figure 1. As seen in Figure 1a, WRF/CMAQ simulations suggest that biomass burning aerosol within the surface layer is mostly limited to the fire source regions. However, as evident in Figure 1b, biomass burning $PM_{2.5}$ in the 800 hPa upper air layer is comparable between the source region and downwind areas over South China. Figure 1c shows that biomass burning DRE is as high as 25 W/m^2 over North Vietnam and South China but less than 15 W/m^2 over fire source countries in PSEA (outlined in red) and follows a pattern more similar to aerosol concentration in the upper air rather than that at the surface layer. The Moderate Resolution Imaging Spectroradiometer (MODIS) cloud fraction shown in Figure 1d suggests that South China experiences more cloud cover where uplifted above cloud biomass burning aerosol can significantly change the DRE. For example, with high biomass burning $PM_{2.5}$ concentration and low cloud fraction (<40%) over Myanmar, aerosol-induced DRE is only 5 W/m^2 because most underlying area is land surface. In contrast, $PM_{2.5}$ is comparatively lower over North Vietnam and the Guangxi Province of China, but cloud fraction in these areas are more than 90%, thus the above cloud aerosol-induced DRE is ~20 W/m^2. Simulations suggest that air temperature at 2 m (T2) is reduced by up to −1 K in PSEA, and the upper air temperature is increased by up to +0.2 K in North Vietnam and South China, as shown in Figures 1e and 1f, respectively. Our modeling estimations are consistent with recent measurement studies (Pani et al., 2016; Tsay et al., 2016).

Figure 1e suggests that surface cooling greatest over PSEA, while Figure 1f indicates upper air warming is more prominent in South China. Therefore, we categorize the IGRA observations as west (sites locations <105°E) and east (sites locations ≥105°E) to represent the PSEA and South China, respectively, and compare the bias between IGRA and ERA in these two areas. Locations of the west and east sites are indicated in Figure 1e by triangles and upside down triangles, respectively, and data averaged at the west and east sites are presented in Figures 1g–1j with solid and dash lines, respectively. We use BIAS to refer the temperature bias between IGRA and ERA, and Sim.ΔT to denote the temperature difference between simulations with and without biomass burning emission. Due to the persistent burning activities in boreal spring over PSEA, March and April are used to represent the biomass burning episode (BIOB, indicated by green lines in Figures 1g and 1f), and the remaining months (January and February, and May–December) are used to represent the non-biomass burning episode (NON-BIOB, indicated by gray lines in Figures 1g, 1i, and 1j). Sim.ΔT is calculated for BIOB, and BIAS is calculated for both BIOB and NON-BIOB.

As shown in Figure 1g, BIAS at the west sites during BIOB is −0.5 K lower than that during NON-BIOB between approximately 1,000 to 975 hPa and +0.2 K higher at 925 hPa. At the east sites, BIAS for BIOB is also lower near the surface and higher in the upper air (850–775 hPa) than BIAS for the NON-BIOB. This episode-dependent BIAS reveals the surface cooling and upper air warming effect of biomass burning aerosol. As presented in Figure 1h. Sim.ΔT exhibits a pattern that is generally consistent with BIAS. Sim.ΔT shows a cooling effect (−0.25 K) at 600 hPa over the west sites probably due to the modulation of latent heat flux (Wu et al., 2011). Sim.ΔT also shows a warming effect (+0.25 K) at 750 hPa over the east sites with no significant corresponding BIAS. The modeling system is self-consistent as it predicts excessive biomass burning aerosol between 750 and 600 hPa, as shown in Figure 1i. The simulated biomass burning aerosol has been thoroughly evaluated for surface concentrations, AOD, and vertical distribution, which suggests reasonable model performance (Dong & Fu, 2015a). In probing further into the inconsistency between BIAS and Sim.ΔT, we find it may be attributed to the discrepancy of cloud simulation. The two-way mode WRF/CMAQ system simulates the direct effect of aerosol only, while the indirect effect affecting cloud condensation nuclei (CCN) or ice nuclei is not represented. In addition, the WRF/CMAQ model underestimates cloud fraction by 12% and cloud top height by 35% (spatial distributions and evaluation statistics of simulated cloud

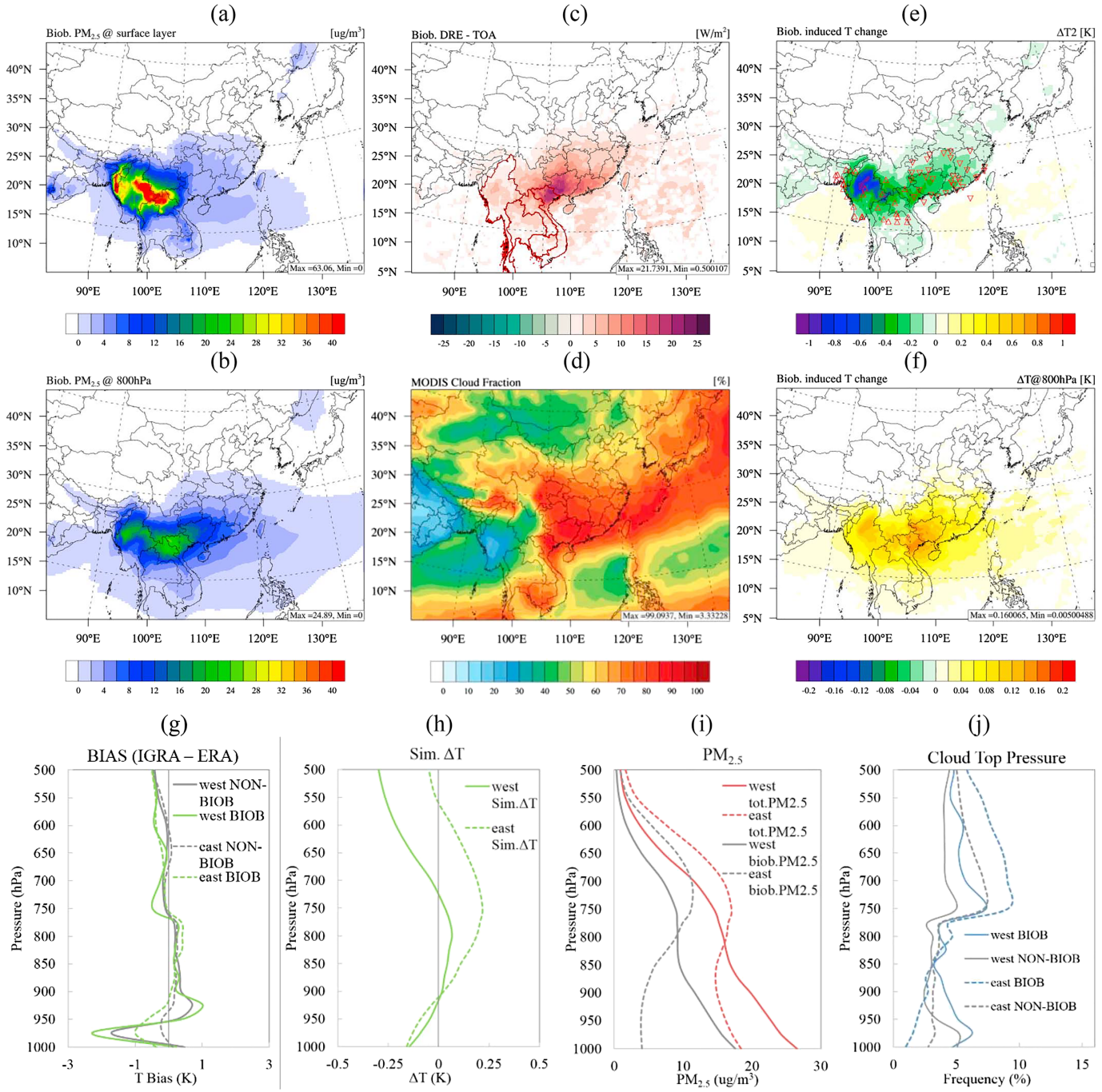

Figure 1. Weather Research and Forecasting/Community Multiscale Air Quality-simulated biomass burning $PM_{2.5}$ concentration at the (a) surface layer and (b) 800-hPa layer; (c) simulated biomass burning direct radiative effect (DRE; Peninsular Southeast Asia countries are outlined in red to indicate the regime of biomass burning emission); (d) cloud fraction from Moderate Resolution Imaging Spectroradiometer (MODIS); simulated biomass burning aerosol-induced temperature change at (e) 2-m height and (f) 800-hPa height; (g) BIAS (temperature bias between Integrated Global Radiosonde Archive [IGRA] observation and European Centre for Medium-Range Weather Forecasts Re-Analysis [ERA] data set, solid line for the west and dash line for the east sites); (h) simulated temperature change due to biomass burning at IGRA sites; (i) simulated total $PM_{2.5}$ and biomass burning $PM_{2.5}$ at IGRA sites; (j) MODIS cloud top frequency at IGRA sites. TOA = top of atmosphere.

cover are presented in Figure S4 and Table S4, respectively). As shown in Figure 1j, frequency of cloud top height derived from MODIS (MOD08) shows a drastic increase at 750 hPa over both west and east sites, which is consistent with pilot studies reporting the persistent stratocumulus cloud deck below 2,000 m (700–800 hPa) in this area (C. Y. Lin et al., 2014; Wood, 2012). Consequently, although WRF/CMAQ may

properly simulate the aerosol concentration and distribution, the significant underestimations of both cloud top height and cloud fraction induces large discrepancies for simulated biomass burning aerosol DRE above 750 hPa.

3.2. Impact of Dust on Regional Climate

DRE of dust are summarized in Figure 2. Dust substantially increases surface PM_{10} by more than 400 $\mu g/m^3$ over Tibet, Talamakan, and the Gobi Desert and also increases the upper air PM_{10} in North China as shown in Figures 2a and 2b. In general, East Asia dust exhibits a cooling effect with DRE as low as -9.5 W/m^2 over Mongolia, North China, South Korea, and Japan as demonstrated in Figure 2c. Figure 2d shows that some areas exhibit positive dust DRE, such as along the north and east boundaries of Tibet Plateau where the MODIS snow and ice product (MOD10CM) indicates the surface is covered by semipersistent snow or ice. Suspended dust above the underlying snow or ice reduces the surface albedo, resulting in a subsequent warming effect. Figures 2e and 2f show the spatial distributions of dust-induced temperature changes at the surface and 700 hPa, respectively. T2 is reduced by -0.5 K near the desert and downwind areas. Elevated dust slightly warms the upper air at 700 hPa by less than +0.2 K, which is in agreement with on-site measurement studies (Clarke et al., 2004; Huebert et al., 2003; Mikami et al., 2006; Shi et al., 2005).

East Asia dust storms usually last for a couple days and may occur in any month of the year (Shao & Dong, 2006). We applied daily average model simulated surface PM_{10} to identify the episode with significant dust impact (DUST) and without significant dust (NON-DUST). At each of the dust-affected IGRA sites (marked by red circles in Figure 2e), days are categorized as DUST if the daily average dust contributed surface PM_{10} is larger than or equal to 5 $\mu g/m^3$ (we also tried 3 and 10 $\mu g/m^3$ as the threshold and found no noticeable difference for BIAS calculation), the remaining days within the simulation period are categorized as NON-DUST. As presented in Figure 2g, BIAS during DUST episodes is larger than that of NON-DUST at 975 and 900 hPa and less than that of NON-DUST at 800–700 hPa, indicating the surface cooling and upper air warming of dust over East Asia. We define the BIAS difference between DUST and NON-DUST to represent the "observed" dust aerosol impact, Obs.ΔT, for comparison with the simulated dust impact, Sim.ΔT, as shown in Figure 2h. The model suggests that dust particles result in cooling that decreases in magnitude from -0.8 K at the surface to 750 hPa where the upper air is warmed by +0.1 K. Obs.ΔT exhibits a similar warming effect in the upper air but with a cooling effect occurring at a lower altitude (1,000–850 hPa) and smaller in magnitude (-0.3 K at the surface).

Driven by frontal systems, East Asia dust storms are apparently closely related with cloud cover. As shown in Figure 2j, cloud top frequency during DUST episodes increase more sharply at 775–750 hPa than during NON-DUST episodes. We also find an interesting positive correlation ($R^2 = 0.56$) between Obs.ΔT and cloud top frequency for DUST episode. At 925 hPa, Obs.ΔT is +0.1 K warmer, and cloud frequency is greater than at 975 and 900 hPa. In contrast, Obs.ΔT is larger in magnitude, but cooling, at 975 and 900 hPa, and cloud top frequency is lower. Figures 2h, 2i, and 2j imply that mixing with fresh hydrophobic dust particles may darken additional clouds at 925 hPa and lead to subsequent warming, while dust particles at 975 and 900 hPa result in cooling by increased scattering due to less cloud cover.

3.3. Correlation Between Aerosol, Temperature Bias, and Cloud Properties

Dry matter (DM) emission from PSEA is used to indicate biomass burning emission intensity. The HD-Index for biomass burning was derived from BIAS between 1,000 to 750 hPa for the west and east IGRA sites, respectively. Since WRF/CMAQ simulated direct effect only, we examined the correlation between DM emission and HD-Index to probe into the overall climate effects of biomass burning aerosol as shown in Figures 3a and 3b.

Daily DM emissions and HD-Index are analyzed from 2003 to 2015 and exhibit correlations at the west and east IGRA sites of 0.56 and 0.25, respectively, revealing a prominent direct impact of biomass burning aerosol over the fire source countries in PSEA but not over downwind areas in South China. We examined the correlation between DM emission and BIAS at altitudes below 600 hPa for each of the east sites but found no significant (>0.3) correlations. Although Figure 1g demonstrates that BIAS for BIOB is obviously different from that of NON-BIOB at the east sites, the low correlation between DM emission and HD-Index suggests that the role of biomass burning aerosol may be more complex than simply altering the RF budget and changing air temperature, such as serving CCN and affecting cloud properties. For the east sites, Figure 1j shows

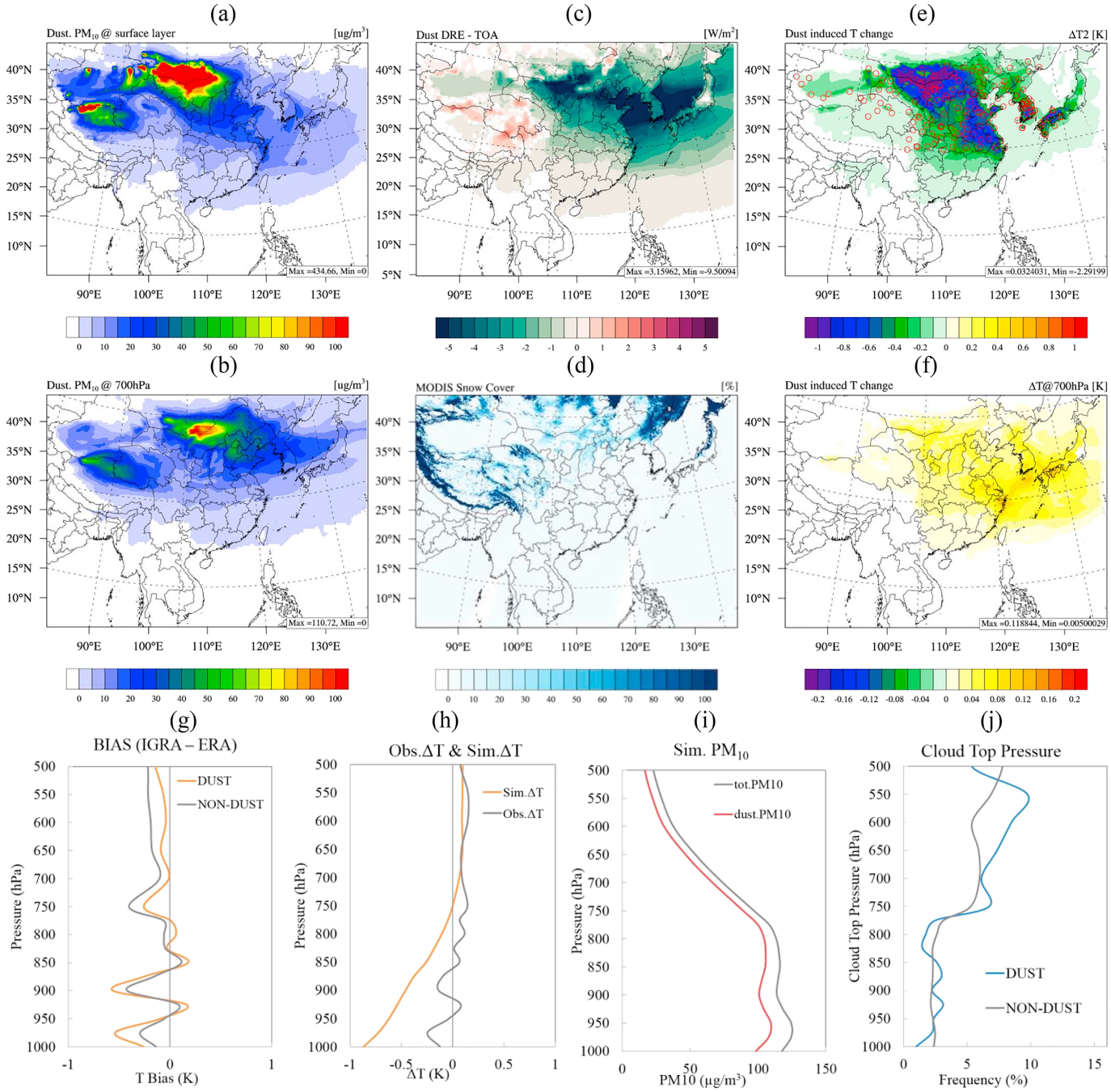

Figure 2. Weather Research and Forecasting/Community Multiscale Air Quality-simulated dust PM_{10} concentration at (a) surface and (b) 700 hPa; (c) simulated dust direct radiative effect (DRE); (d) snow coverage from Moderate Resolution Imaging Spectroradiometer (MODIS); simulated dust-induced temperature change at (e) 2 m and (f) 700 hPa; (g) BIAS (site locations indicated in Figure 2e); (h) simulated temperature change due to dust at Integrated Global Radiosonde Archive (IGRA) sites; (i) simulated total PM_{10} and dust PM_{10} at IGRA sites; (j) MODIS cloud top frequency at IGRA sites. TOA = top of atmosphere.

substantially lower cloud top frequency at altitudes below 850 hPa and higher cloud top frequency above 750 hPa during for BIOB. Biomass burning introduces excess fine-size particles into the upper air, especially over South China, which may change CCN or ice droplets and subsequently affect cloud activities (Jiang et al., 2018; Wu et al., 2012, 2015; Zhao, Jiang et al., 2018; Zhao, Gu et al., 2018). However, we find no noticeable correlation (>0.1) between DM emission and cloud properties (i.e., cloud top temperature, cloud effective radius, cloud top pressure, and cloud optical depth) either for 2003–2015. Since the correlation coefficient only depicts the monotonic relationship between variables, we

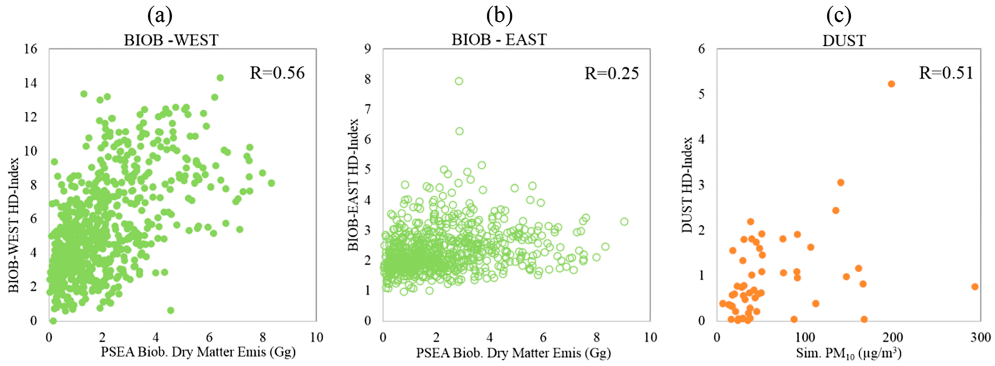

Figure 3. Scatter plots of Peninsular Southeast Asia (PSEA) biomass burning dry matter emission versus HD-Index for BIOB at the (a) west and (b) east Integrated Global Radiosonde Archive sites; (c) scatter plot of PM_{10} concentration versus HD-Index for DUST.

recommend that a more comprehensive statistical analysis might be helpful in future research to explore the indirect climate effects of biomass burning aerosol over South China.

As shown in Figure 3c, HD-Index for dust was calculated with BIAS below 700-hPa altitude and compared with the simulated surface PM_{10} concentration, used to indicate the dust intensity, revealing a correlation of 0.51, indicating the important direct effect of dust aerosol. We also examined the relationship between simulated PM_{10} and cloud properties but find no noticeable (>0.1) correlation.

3.4. DRE of Dust and Biomass Burning Under Coexist Condition

Biomass burning aerosols and dust can both be present over the southeast coast of China in boreal spring (Dong et al., 2018). In this section, we examine the overall DRE change resulting from the simultaneous presence of both biomass burning and dust aerosols, which to our knowledge has never been investigated.

The majority of biomass burning plumes from PSEA usually remain within 2–5 km above the surface in Taiwan. During occasional dust storms originating from the Taklamakan or Gobi deserts, biomass burning plumes could be pushed down to ~1.5 km and mix with dust, driven by large scale subsidence (Dong et al., 2018). Figure 4a presents BIAS at Taipei (24.97°N, 121.18°E) with IGRA and ERA data analyzed from 2005 through 2012 for the coexistence of biomass and dust aerosols (Coexist), biomass burning only (Biob), and other (Other) episodes, respectively (detailed episodes descriptions are found in supplemental Text S5 and Table S5). Coexist exhibits substantially larger negative BIAS at the surface layer and larger positive BIAS at 775 hPa compared with Biob. The surface cooling and upper air warming effects are both significantly intensified under the Coexist condition compared to the effects of pure biomass burning aerosol, shown in Figure 1g, and pure dust, shown in Figure 2g. The vertical profiles of BIAS are generally consistent with the normalized relative backscatter (NRB) coefficient shown in Figure 4b. NRB measurements are collected with the NASA Micro-Pulse Lidar system, and the data are analyzed for the same period and episodes. Figure 4b clearly demonstrates that from the surface to 4 km (~600 hPa) Coexist aerosol concentrations are substantially higher than those during the other two episodes. Figure 4c shows the relationship between HD-Index calculated with BIAS from 900 to 600 hPa (layers below 900-hPa altitude are excluded to filter out the influence of local anthropogenic aerosol) and NRB averaged over 1–4 km. The correlations between HD-Index and NRB are 0.55, 0.18, and 0.13 for Coexist, Biob, and Other, respectively, suggesting the prominent direct effect of dust and biomass burning under the coexist condition. The low correlation coefficient for Biob at Taipei suggests biomass burning aerosol may play a more complex role than directly altering air temperature after long-range transport, which is consistent with the result discussed regarding Figure 3b.

As shown in Figure 4d, we also calculate the aerosol direct radiative efficiency $E\tau$ (Yu et al., 2006) as the aerosol-induced change in DRE divided by the aerosol-induced change in AOD. Biomass burning shows higher warming efficiency over the PSEA fire emission source region (west IGRA sites) than over the downwind region in South China (east IGRA sites). $E\tau$ was estimated for clear sky only due to the availability of MODIS AOD product. Decreases of dust and biomass burning during the long-range transport shall be due to the calculation of shortwave flux by Rapid Radiative Transfer Model for global circulation models

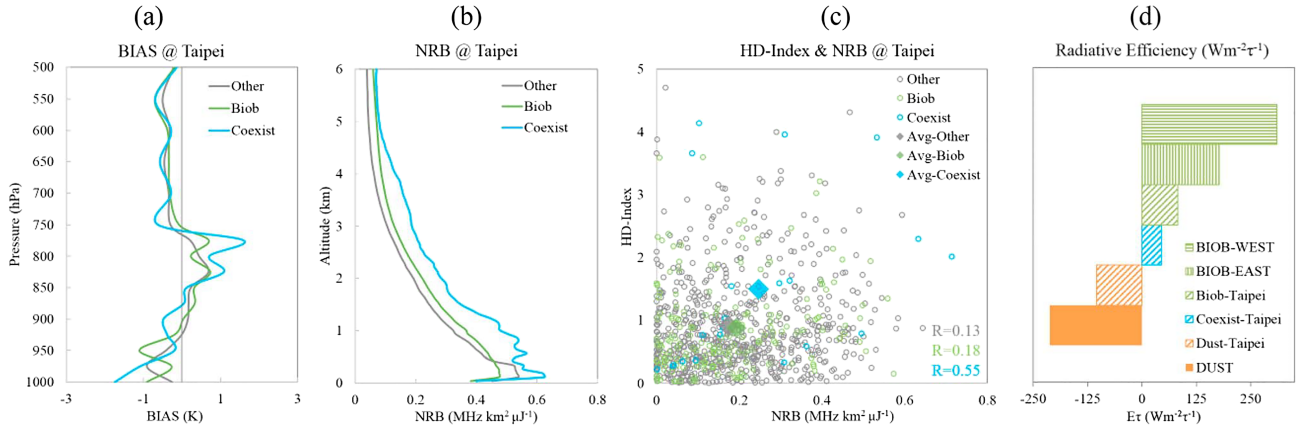

Figure 4. (a) BIAS, (b) normalized relative backscatter (NRB), and (c) scatter plots of HD-Index and NRB at Taipei. Gray, green, and blue lines and circles represent the Other, Biob, and Coexist episodes, respectively. Solid diamonds in (c) represent the averages of each episodes. (d) Aerosol radiative efficiency for biomass burning at the west (green box with horizontal lines) and east (green box with vertical lines) Integrated Global Radiosonde Archive sites, at Taipei (green box with diagonal lines), for dust at the North China Integrated Global Radiosonde Archive sites (solid orange), at Taipei (orange box with diagonal lines), and for the coexist condition at Taipei.

for 0.2–12.2 μm, but AOD was for 0.55 μm; thus, the deposition of coarse particles affected calculation of DRE but had little impact on AOD. At Taipei, biomass burning Eτ is decreased by 75% during the long-range transport from PSEA. Dust shows a stronger cooling effect over North China, and dust Eτ is decreased by 50% during transport to Taipei. Under the coexist condition, the combined effect of biomass burning and dust aerosols is a slight net warming effect with positive Eτ value.

4. Summary

We applied the WRF/CMAQ model to estimate the direct effect of dust and biomass burning aerosols over East Asia. We find dominant cooling effects of dust over Mongolia, North China, South Korea, and Japan, with a few exceptions around the Tibet Plateau due to the semipersistent snow or ice land cover. Biomass burning is found to have a warming effect of 5–10 W/m^2 in PSEA and 10–20 W/m^2 in South China, indicating a more significant impact over the downwind area than over the fire source area. Dust and biomass burning are found to cool the near surface air and warm the upper air where excess aerosols are found, as demonstrated by both simulations and the bias between reanalysis data and observations. It shall be noticed that the aerosol DRE reported in this study represent the assessment for March and April only. The correlations between HD-Index and aerosol intensities become significantly smaller over long-range transport areas for both dust and biomass burning, suggesting that HD-Index may not be able to inform the aerosol effect for remote downwind areas. The net direct forcing effect of dust and biomass burning aerosols under coexisting conditions is examined for the first time at Taipei. Compared to pure dust or biomass burning aerosol, the surface cooling and upper air warming effect are both intensified under the coexist condition with a slight overall warming effect. By investigating the aerosol direct radiative efficiencies for dust and biomass burning in the near source regions (i.e., North China and PSEA) and downwind regions (i.e., South China and Taipei), we also find these efficiencies decrease in magnitude with long-range transport. The results of this study provide a baseline assessment of the direct effect and impact of biomass burning and dust aerosols on regional climate over East Asia and suggests the need for future research to reevaluate their impacts on regional climate over cloudy areas. The inconsistency between model simulation and the HD-Index method also implies an urgent need to improve the simulation of cloud cover within regional climate modeling.

Acknowledgments
We greatly thank the Joint Institute for Computational Sciences of the University of Tennessee and Oak Ridge National Laboratory for providing the computational resources used in this research. The GFED data can be found at https://www.globalfiredata.org/data.html; the IGRA Radiosonde data can be downloaded from https://www1.ncdc.noaa.gov/pub/data/igra/; the ERA reanalysis data are available at https://www.ecmwf.int/en/forecasts/datasets/reanalysis-datasets/era-interim/; MODIS products can be found at https://modis.gsfc.nasa.gov/data/.

References

Akagi, S. K., Yokelson, R. J., Wiedinmyer, C., Alvarado, M. J., Reid, J. S., Karl, T., et al. (2011). Emission factors for open and domestic biomass burning for use in atmospheric models. *Atmospheric Chemistry and Physics*, *11*(9), 4039–4072. https://doi.org/10.5194/acp-11-4039-2011

Appel, K. W., Napelenok, S. L., Foley, K. M., Pye, H. O. T., Hogrefe, C., Luecken, D. J., et al. (2017). Description and evaluation of the Community Multiscale Air Quality (CMAQ) modeling system version 5.1. *Geoscientific Model Development*, *10*(4), 1703–1732. https://doi.org/10.5194/gmd-10-1703-2017

Clarke, A. D., Shinozuka, Y., Kapustin, V. N., Howell, S., Huebert, B., Doherty, S., et al. (2004). Size distributions and mixtures of dust and black carbon aerosol in Asian outflow: Physiochemistry and optical properties. *Journal of Geophysical Research*, *109*, D15S09. https://doi.org/10.1029/2003JD004378

Dong, X. Y., & Fu, J. S. (2015a). Understanding interannual variations of biomass burning from Peninsular Southeast Asia, part I: Model evaluation and analysis of systematic bias. *Atmospheric Environment*, *116*, 293–307.

Dong, X. Y., & Fu, J. S. (2015b). Understanding interannual variations of biomass burning from Peninsular Southeast Asia, part II: Variability and different influences in lower and higher atmosphere levels. *Atmospheric Environment*, *115*, 9–18.

Dong, X. Y., Fu, J. S., Huang, K., Lin, N. H., Wang, S. H., & Yang, C. E. (2018). Analysis of the co-existence of long-range transport biomass burning and dust in the subtropical West Pacific region. *Scientific Reports*, *8*.

Dong, X. Y., Fu, J. S., Huang, K., Tong, D., & Zhuang, G. S. (2016). Model development of dust emission and heterogeneous chemistry within the Community Multiscale Air Quality modeling system and its application over East Asia. *Atmospheric Chemistry and Physics*, *16*(13), 8157–8180.

Forster, P. M. D., & Taylor, K. E. (2006). Climate forcings and climate sensitivities diagnosed from coupled climate model integrations. *Journal of Climate*, *19*(23), 6181–6194.

Gan, C. M., Pleim, J., Mathur, R., Hogrefe, C., Long, C. N., Xing, J., et al. (2015). Assessment of long-term WRF-CMAQ simulations for understanding direct aerosol effects on radiation "brightening" in the United States. *Atmospheric Chemistry and Physics*, *15*(21), 12,193–12,209. https://doi.org/10.5194/acp-15-12193-2015

Gu, Y., Liou, K. N., Xue, Y., Mechoso, C. R., Li, W., & Luo, Y. (2006). Climatic effects of different aerosol types in China simulated by the UCLA general circulation model. *Journal of Geophysical Research*, *111*, D15201. https://doi.org/10.1029/2005JD006312

Gu, Y., Xue, Y., De Sales, F., & Liou, K. N. (2016). A GCM investigation of dust aerosol impact on the regional climate of North Africa and South/East Asia. *Climate Dynamics*, *46*(7-8), 2353–2370.

Haywood, J., Francis, P., Dubovik, O., Glew, M., & Holben, B. (2003). Comparison of aerosol size distributions, radiative properties, and optical depths determined by aircraft observations and Sun photometers during SAFARI 2000. *Journal of Geophysical Research*, *108*(D13), 8471. https://doi.org/10.1029/2002JD002250

Heald, C. L., Ridley, D. A., Kroll, J. H., Barrett, S. R. H., Cady-Pereira, K. E., Alvarado, M. J., & Holmes, C. D. (2014). Contrasting the direct radiative effect and direct radiative forcing of aerosols. *Atmospheric Chemistry and Physics*, *14*(11), 5513–5527.

Hsu, N. C., Herman, J. R., & Tsay, S. C. (2003). Radiative impacts from biomass burning in the presence of clouds during boreal spring in southeast Asia. *Geophysical Research Letters*, *30*(5), 1224. https://doi.org/10.1029/2002GL016485

Hsu, N. C., Herman, J. R., & Weaver, C. (2000). Determination of radiative forcing of Saharan dust using combined TOMS and ERBE data. *Journal of Geophysical Research*, *105*(D16), 20,649–20,661.

Huang, X., Wang, Z. L., & Ding, A. J. (2018). Impact of aerosol-PBL interaction on haze pollution: Multiyear observational evidences in North China. *Geophysical Research Letters*, *45*, 8596–8603. https://doi.org/10.1029/2018GL079239

Huebert, B. J., Bates, T., Russell, P. B., Shi, G. Y., Kim, Y. J., Kawamura, K., et al. (2003). An overview of ACE-Asia: Strategies for quantifying the relationships between Asian aerosols and their climatic impacts. *Journal of Geophysical Research*, *108*(D23), 8633. https://doi.org/10.1029/2003JD003550

Huneeus, N., Schulz, M., Balkanski, Y., Griesfeller, J., Prospero, J., Kinne, S., et al. (2011). Global dust model intercomparison in AeroCom phase I. *Atmospheric Chemistry and Physics*, *11*(15), 7781–7816. https://doi.org/10.5194/acp-11-7781-2011

Jiang, J. H., Su, H., Huang, L., Wang, Y., Massie, S., Zhao, B., et al. (2018). Contrasting effects on deep convective clouds by different types of aerosols. *Nature Communications*, *9*(1), 3874. https://doi.org/10.1038/s41467-018-06280-4

Kaufman, Y. J., & Koren, I. (2006). Smoke and pollution aerosol effect on cloud cover. *Science*, *313*(5787), 655–658.

Keil, A., & Haywood, J. M. (2003). Solar radiative forcing by biomass burning aerosol particles during SAFARI 2000: A case study based on measured aerosol and cloud properties. *Journal of Geophysical Research*, *108*(D13), 8467. https://doi.org/10.1029/2002JD002315

Kok, J. F., Ridley, D. A., Zhou, Q., Miller, R. L., Zhao, C., Heald, C. L., et al. (2017). Smaller desert dust cooling effect estimated from analysis of dust size and abundance. *Nature Geoscience*, *10*(4), 274–278. https://doi.org/10.1038/ngeo2912

Koren, I., Martins, J. V., Remer, L. A., & Afargan, H. (2008). Smoke invigoration versus inhibition of clouds over the Amazon. *Science*, *321*(5891), 946–949. https://doi.org/10.1126/science.1159185

Lin, C. Y., Zhao, C., Liu, X. H., Lin, N. H., & Chen, W. N. (2014). Modelling of long-range transport of Southeast Asia biomass-burning aerosols to Taiwan and their radiative forcings over East Asia. *Tellus Series B-Chemical and Physical Meteorology*, *66*(1). https://doi.org/10.3402/tellusb.v66.23733

Lin, N. H., Tsay, S. C., Maring, H. B., Yen, M. C., Sheu, G. R., Wang, S. H., et al. (2013). An overview of regional experiments on biomass burning aerosols and related pollutants in Southeast Asia: From BASE-ASIA and the Dongsha Experiment to 7-SEAS. *Atmospheric Environment*, *78*, 1–19. https://doi.org/10.1016/j.atmosenv.2013.04.066

Mahowald, N. M., Muhs, D. R., Levis, S., Rasch, P. J., Yoshioka, M., Zender, C. S., & Luo, C. (2006). Change in atmospheric mineral aerosols in response to climate: Last glacial period, preindustrial, modern, and doubled carbon dioxide climates. *Journal of Geophysical Research*, *111*, D10202. https://doi.org/10.1029/2005jd006653

Mikami, M., Shi, G. Y., Uno, I., Yabuki, S., Iwasaka, Y., Yasui, M., et al. (2006). Aeolian dust experiment on climate impact: An overview of Japan-China joint project ADEC. *Global and Planetary Change*, *52*(1-4), 142–172. https://doi.org/10.1016/j.gloplacha.2006.03.001

Pani, S. K., Wang, S. H., Lin, N. H., Lee, C. T., Tsay, S. C., Holben, B. N., et al. (2016). Radiative effect of springtime biomass-burning aerosols over Northern Indochina during 7-SEAS/BASELInE 2013 campaign. *Aerosol and Air Quality Research*, *16*(11), 2802–2817. https://doi.org/10.4209/aaqr.2016.03.0130

Reid, J. S., Hyer, E. J., Prins, E. M., Westphal, D. L., Zhang, J., Wang, J., et al. (2009). Global monitoring and forecasting of biomass-burning smoke: Description of and lessons from the Fire Locating and Modeling of Burning Emissions (FLAMBE) program. *IEEE Journal of Selected Topics in Applied Earth Observations and Remote Sensing*, *2*(3), 144–162. https://doi.org/10.1109/JSTARS.2009.2027443

Shao, Y., & Dong, C. H. (2006). A review on East Asian dust storm climate, modelling and monitoring. *Global and Planetary Change*, *52*(1-4), 1–22.

Shi, Z. B., Shao, L. T., Jones, T. P., & Lu, S. L. (2005). Microscopy and mineralogy of airborne particles collected during severe dust storm episodes in Beijing, China. *Journal of Geophysical Research*, *110*, D01303. https://doi.org/10.1029/2004JD005073

Tsay, S. C., Hsu, N. C., Lau, W. K. M., Li, C., Gabriel, P. M., Ji, Q., et al. (2013). From BASE-ASIA toward 7-SEAS: A satellite-surface perspective of boreal spring biomass-burning aerosols and clouds in Southeast Asia. *Atmospheric Environment*, *78*, 20–34. https://doi.org/10.1016/j.atmosenv.2012.12.013

Tsay, S. C., Maring, H. B., Lin, N. H., Buntoung, S., Chantara, S., Chuang, H. C., et al. (2016). Satellite-surface perspectives of air quality and aerosol-cloud effects on the environment: An overview of 7-SEAS/BASELInE. *Aerosol and Air Quality Research*, *16*(11), 2581–2602. https://doi.org/10.4209/aaqr.2016.08.0350

van der Werf, G. R., Randerson, J. T., Giglio, L., van Leeuwen, T. T., Chen, Y., Rogers, B. M., et al. (2017). Global fire emissions estimates during 1997-2016. *Earth System Science Data*, *9*(2), 697–720. https://doi.org/10.5194/essd-9-697-2017

Wilcox, E. M. (2012). Direct and semi-direct radiative forcing of smoke aerosols over clouds. *Atmospheric Chemistry and Physics*, *12*(1), 139–149. https://doi.org/10.5194/acp-12-139-2012

Wong, D. C., Pleim, J., Mathur, R., Binkowski, F., Otte, T., Gilliam, R., et al. (2012). WRF-CMAQ two-way coupled system with aerosol feedback: Software development and preliminary results. *Geoscientific Model Development*, *5*(2), 299–312. https://doi.org/10.5194/gmd-5-299-2012

Wood, R. (2012). Stratocumulus clouds. *Monthly Weather Review*, *140*(8), 2373–2423.

Woodward, S., Roberts, D. L., & Betts, R. A. (2005). A simulation of the effect of climate change-induced desertification on mineral dust aerosol. *Geophysical Research Letters*, *32*, L18810. https://doi.org/10.1029/2005GL023482

Wu, L., Su, H., Jiang, J. H., & Read, W. G. (2012). Hydration or dehydration: Competing effects of upper tropospheric cloud radiation on the TTL water vapor. *Atmospheric Chemistry and Physics*, *12*(16), 7727–7735.

Wu, L. T., Li, J. L. F., Pi, C. J., Yu, J. Y., & Chen, J. P. (2015). An observationally based evaluation of WRF seasonal simulations over the Central and Eastern Pacific. *Journal of Geophysical Research: Atmospheres*, *120*, 10,664–10,680. https://doi.org/10.1002/2015JD023561

Wu, L. T., Su, H., & Jiang, J. H. (2011). Regional simulations of deep convection and biomass burning over South America: 1. Model evaluations using multiple satellite data sets. *Journal of Geophysical Research*, *116*, D17208. https://doi.org/10.1029/2011jd016105

Yu, H., Kaufman, Y. J., Chin, M., Feingold, G., Remer, L. A., Anderson, T. L., et al. (2006). A review of measurement-based assessments of the aerosol direct radiative effect and forcing. *Atmospheric Chemistry and Physics*, *6*(3), 613–666. https://doi.org/10.5194/acp-6-613-2006

Zhao, B., Gu, Y., Liou, K. N., Wang, Y., Liu, X., Huang, L., et al. (2018). Type-dependent responses of ice cloud properties to aerosols from satellite retrievals. *Geophysical Research Letters*, *45*, 3297–3306. https://doi.org/10.1002/2018GL077261

Zhao, B., Jiang, J. H., Diner, D. J., Su, H., Gu, Y., Liou, K. N., et al. (2018). Intra-annual variations of regional aerosol optical depth, vertical distribution, and particle types from multiple satellite and ground-based observational datasets. *Atmospheric Chemistry and Physics*, *18*(15), 11,247–11,260. https://doi.org/10.5194/acp-18-11247-2018